Bulletin of the Seismological Society of America, Vol. 86, No. 6, pp. 1704–1713, December 1996

Shallow Velocity Structure and Poisson's Ratio at the Tarzana, California, Strong-Motion Accelerometer Site

by R. D. Catchings and W. H. K. Lee

Abstract The 17 January 1994, Northridge, California, earthquake produced strong ground shaking at the Cedar Hills Nursery (referred to here as the Tarzana site) within the city of Tarzana, California, approximately 6 km from the epicenter of the mainshock. Although the Tarzana site is on a hill and is a rock site, accelerations of approximately 1.78 *g* horizontally and 1.2 *g* vertically at the Tarzana site are among the highest ever instrumentally recorded for an earthquake. To investigate possible site effects at the Tarzana site, we used explosive-source seismic refraction data to determine the shallow (<70 m) *P*- and *S*-wave velocity structure. Our seismic velocity models for the Tarzana site indicate that the local velocity structure may have contributed significantly to the observed shaking. *P*-wave velocities range from 0.9 to 1.65 km/sec, and *S*-wave velocities range from 0.20 and 0.6 km/sec for the upper 70 m. We also found evidence for a local *S*-wave low-velocity zone (LVZ) beneath the top of the hill. The LVZ underlies a CDMG strong-motion recording site at depths between 25 and 60 m below ground surface (BGS). Our velocity model is consistent with the near-surface (<30 m) *P*- and *S*-wave velocities and Poisson's ratios measured in a nearby (<30 m) borehole. High Poisson's ratios (0.477 to 0.494) and *S*-wave attenuation within the LVZ suggest that the LVZ may be composed of highly saturated shales of the Modelo Formation. Because the lateral dimensions of the LVZ approximately correspond to the areas of strongest shaking, we suggest that the highly saturated zone may have contributed to localized strong shaking. Rock sites are generally considered to be ideal locations for site response in urban areas; however, localized, highly saturated rock sites may be a hazard in urban areas that requires further investigation.

Introduction

In order to investigate the causes of large accelerations observed at the Cedar Hills Nursery (referred to here as the Tarzana site) in Tarzana, California, during the 1994 Northridge, California, earthquake, the U.S. Geological Survey recorded aftershocks (Lee *et al.,* 1994) and an active-source seismic survey over the Tarzana site in February 1994. In this article, we present a model of the shallow (<70 m) compressional- and shear-wave velocity structure and Poisson's ratio, derived from explosive-source data, beneath the Tarzana site.

During the 17 January 1994, Northridge, California, earthquake, numerous areas throughout the Los Angeles region experienced strong shaking. Some of the strongest shaking occurred at Tarzana, California, a Los Angeles suburb located in the southwestern San Fernando Valley approximately 6 km from the 17 January 1994 Northridge epicenter (Fig. 1). A California Division of Mines and Geology (CDMG) strong-motion accelerometer, located at the Cedar Hills Nursery in Tarzana, recorded one of the highest acceleration measurements (1.78 *g* horizontally and 1.2 *g* vertically) that has been instrumentally recorded for an earthquake (Shakal *et al.,* 1994). The severity of shaking at the Tarzana CDMG site was unexpected because the site is underlain by bedrock within a few meters of the surface, unlike many soft-sediment sites that exhibit such amplified ground motion. Furthermore, the strong shaking recorded at the CDMG site was locally confined because much less intense shaking was observed at distances as little as 150 m from the CDMG site, as evidenced by mobile homes perched on wooden pillars and stacked clay pottery that was left intact.

A contributor to the strong shaking at the Tarzana site might have been the elevated topography, as the CDMG site is located on an 18-m-high hill that is about 500 m long and about 200 m wide (Fig. 2). Elevated topography is known to amplify shaking, but Spudich *et al.* (1996) concluded that the strongest directional topographic effect does not fully account for the measured amplitudes at the top of the hill relative to those at the base of the hill during the mainshock.

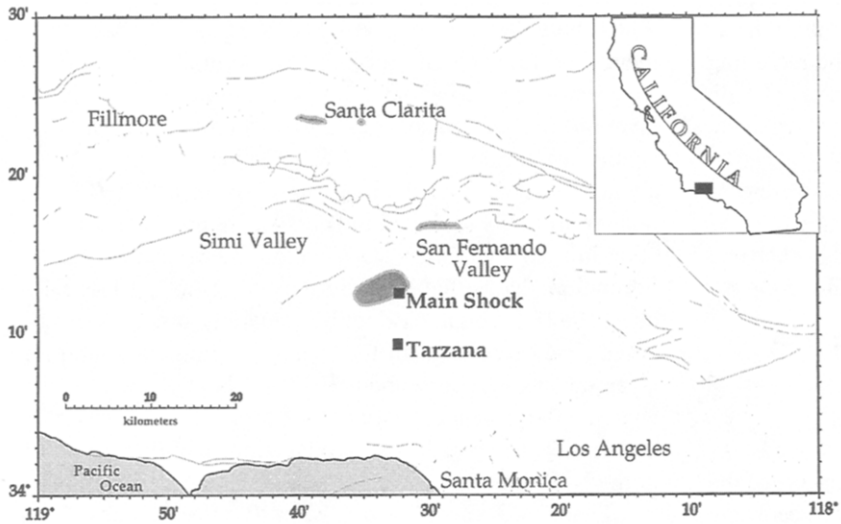

Figure 1. Map of the southern California region showing the city of Tarzana, California, relative to the mainshock of the 17 January 1994 Northridge earthquake and selected surrounding cities. The double-shaded areas show locations where ground breakage occurred during the 1994 mainshock. The light-shaded lines represent mapped faults in the area.

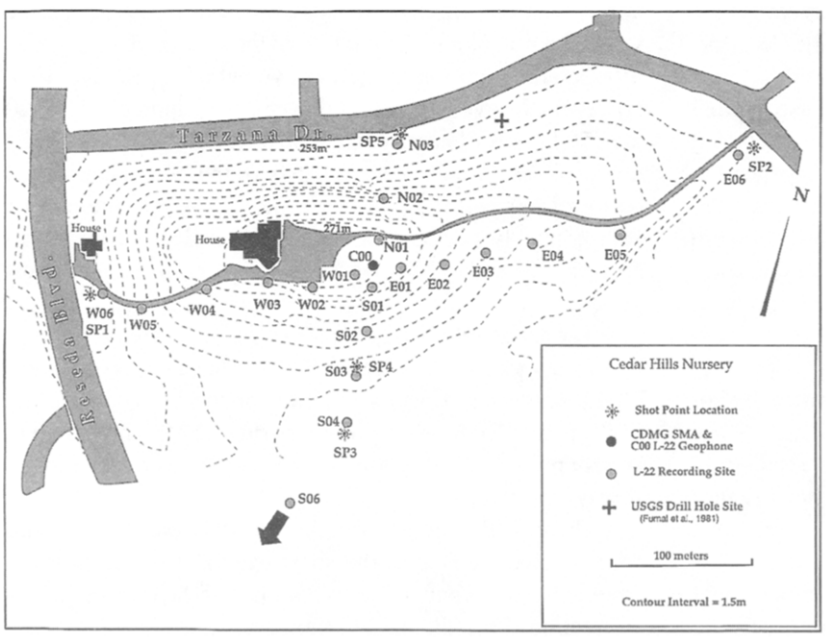

Figure 2. Topographic map of the area surrounding the Cedar Hills Nursery, where a California Division of Mines and Geology (CDMG) strong-motion accelerometer recorded exceptional accelerations during the 17 January 1994 Northridge earthquake. Recording sites labeled "N0# and S0#" refer to the north–south recording array, and recording sites labeled "E0# and W0#" refer to the east–west recording array. Site C00 refers to the location of both the CDMG strong-motion accelerometer and the location of our L-22 recording site.

Spudich *et al.* further conclude that the internal structure of the hill likely enhances the strong shaking. The intense shaking at the Tarzana site is a condition of the site and not peculiar to the Northridge earthquake because unusually strong ground motion was also observed there during the 1987 Whittier-Narrows earthquake (Shakal *et al.*, 1988) and during most aftershocks following both mainshocks.

The Tarzana site is principally composed of shales or weathered shales of the Modello Formation (Hoots, 1931; Dibblee, 1992) at the surface. Fumal *et al.* (1981) described the upper 6 m at a nearby borehole as "silty clay loam, olive, very stiff, slight plasticity, and deeply to moderately weathered shale with shale parting visible." From 6 to 30 m, Fumal *et al.* (1981) described drill samples as "shale, black, soft to firm, very close horizontal parting, close to very close fracture spacing, and fresh." Rock exposures are particularly noticeable at the surface on the south side of the hill.

Seismic Survey

For both the aftershock and the active-source surveys, the seismic data were recorded on a 64-channel, 16-bit PC recording system described by Lee (1989) and Lee and Dodge (1992). A 30-Hz, high-cut filter and a sampling rate of 200 samples/sec were used. Twenty-one 2-Hz, L-22 geophones were buried at a depth of about 0.3 m and connected via cable to the recording array. The geophones were arranged in a cross pattern, with 13 geophones nominally spaced about 15 to 50 m apart along the length of the hill (approximate E–W direction) and 9 geophones spaced about

15 to 50 m apart across the hill (approximate N–S direction) (Fig. 2). One recording site, C00, was co-located with the CDMG strong ground motion accelerometer. The recording sites and the active-source shot points were surveyed with an electronic distance meter, yielding vertical and horizontal accuracies of a few centimeters.

For the active-source survey, seismic sources were generated by buried (~1.5 m deep) one-pound explosions of ammonium nitrate. A seismic source was placed at each end of the array, with an additional source located along the N–S array at the S03 recording station (Fig. 2).

Data and Modeling Approach

Both the N–S and E–W arrays recorded all sources. As a result, all sources were recorded in the plane of one of the recording arrays and perpendicular to the other recording array. A total of 630 vertical- and horizontal-component seismograms was recorded. Because the one-pound shots were particularly energetic, some of the seismic records near the shot points were clipped, and valuable amplitude information was lost.

A shear-wave source (Lui *et al.,* 1988) was also applied at each shot point, but those shear-wave data were not used in this analysis. Instead, the one-pound blasts generated high-amplitude shear waves that were recorded across the length of each array. Thus, both *P*- and *S*-wave data were available from the same sources and were used in this analysis. Both *P* and *S* waves were picked on vertical-component shot gathers, and *S*-wave picks were checked on horizontal-component shot gathers for accuracy.

One-dimensional modeling of the data from each shot point was accomplished using software by Luetgert (1988). In the one-dimensional modeling approach, observed travel times are matched to calculated travel times without regard to lateral changes in velocity or elevation. Lateral variations in velocities and depths between the shot points were assumed to be linear in developing an initial two-dimensional (2D) velocity model, and the topography along the seismic lines was included. Two-dimensional modeling was accomplished using a seismic modeling routine called MacRay (Luetgert, 1992), which uses ray theory (Cerveny *et al.,* 1977) in a trial-and-error approach. Topography and lateral changes in velocity were included in the calculated travel times. We chose this forward-modeling approach because we had too few shot points for inversion and because MacRay permitted determination of *S*-wave velocities and Poisson's ratios from the same model. Seismic velocities and velocity structures were altered until the calculated arrivals correlated with the observed arrivals to within an acceptable error, typically about 5 ms for *P* waves.

Preferred Velocity Model

Our preferred velocity models and models of Poisson's ratio consist of three layers (Figs. 3 and 4) with lateral variations in velocity. Layer one ranges in thickness from about 20 to about 40 m in thickness and consists of surface sediments and low-velocity rock that range in *P*-wave velocity from about 0.95 to about 1.1 km/sec. *S*-wave velocities in layer one range from about 0.35 to 0.44 km/sec, but can vary significantly. Some *P*- and *S*-wave velocities appear to be about 5 to 20% higher along the E–W direction (Fig. 3) relative to the N–S direction (Fig. 4); we attribute the variation in velocity to anisotropy within the Miocene Modello Formation shales that underlie the hill (Hoots, 1931; Dibblee, 1992), as higher velocities generally occur along the strike (E–W direction) of the shale. The Poisson's ratio for layer one varies from about 0.38 to about 0.43. As with velocity, there are local variations. Poisson's ratios generally differ with the direction of propagation, with higher ratios in the N–S direction.

Layer two varies vertically in *P*-wave velocity from about 1.45 to about 1.65 km/sec, and varies in thickness from about 30 to about 80 m. The depth to the base of layer two is not well constrained but is best determined beneath the top of the hill. Our interpretation of the seismic data suggests little lateral variation in the *P*-wave velocities in layer two; however, *S*-wave velocities in layer 2 vary appreciably (0.20 to 0.54 km/sec) laterally. Generally, the *S*-wave velocity is highest beneath the base and flanks of the hill and appear to be lower beneath the top of the hill, where we interpret an approximately 100-m-wide *S*-wave low-velocity zone (LVZ) at depths of about 25 to about 60 m BGS in the east–west direction.

The modeled Poisson's ratios of layer 2 are high, ranging from about 0.433 to about 0.491. We calculate the highest Poisson's ratio near the center of the hill, beneath the C00 or the CDMG strong-motion site. The high ratios are largely reflective of the low *S*-wave velocities relative to the *P*-wave velocities.

There is limited information on the velocity structure beneath layer 2. Due to the short length of the N–S array, there are few raypaths that travel through layer 3 in the N–S direction (Figs. 5b and 7b); however, seismic energy penetrates more deeply (~80 m) along the longer E–W array (Figs. 5b). The geometry of layer 3 is not well constrained, but the modeled geometry explains refracted first and secondary arrivals. The velocities and ratios at the base of layer 3 are not well constrained and are presented here for modeling purposes only. The modeled *P*-wave velocities for uppermost layer 3 range from about 1.8 to about 2.0 km/sec, with higher velocities measured along the E–W direction, along the strike of the shale.

Resolutions

Resolution in our model is limited because of coarse (15-m minimum) sampling of the seismic wave field, the wide spacing of the seismic sources, and the limited bandwidth (<30 Hz) of the recorded data. Using the highest velocity (*P* wave = 1.65 km/sec; *S* wave = 0.76 km/sec) for layer 2 and the high-cut frequency filter (30 Hz) of our ac-

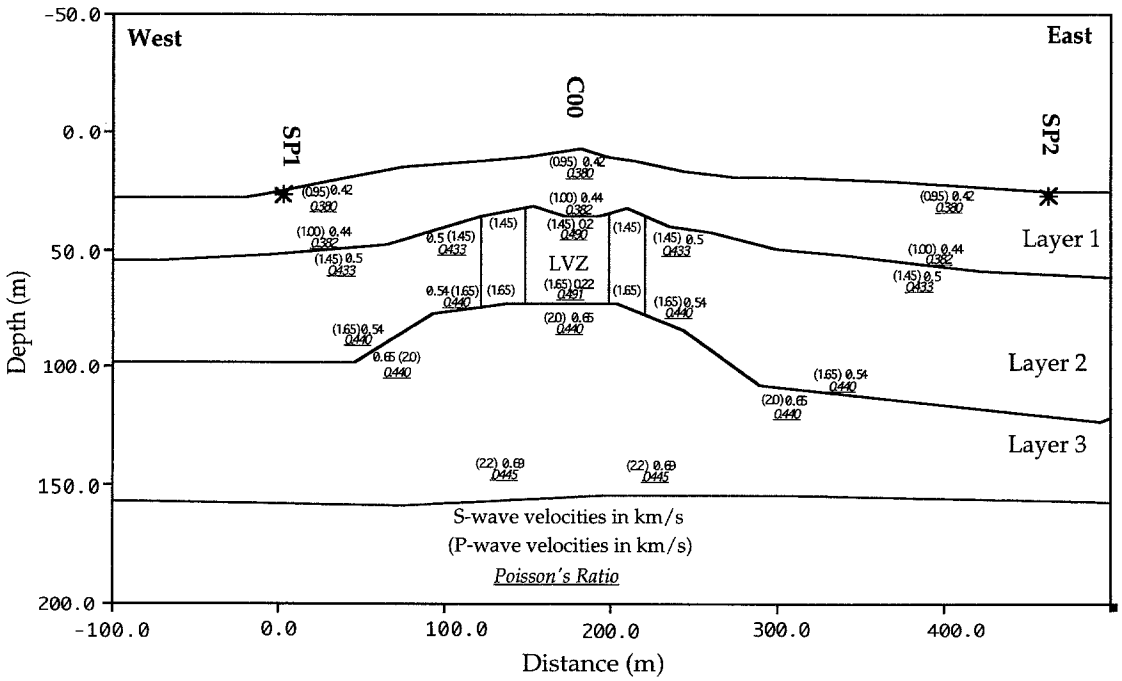

Figure 3. Velocity model (*P* and *S* wave) and Poisson ratio model along the east–west recording array (see Fig. 2). *P*-wave velocities are in parentheses and Poisson's ratios are underlined. C00 refers to the recording site co-located with the CDMG strong-motion accelerometer. Shot points denoted by SP#. Depth is relative to a datum equal to the highest elevation. Unusually high Poisson's ratios and low *S*-wave velocities are observed within layer 2, beneath the C00 site.

quisition system, the maximum error between observed and calculated arrivals corresponds to a depth error of about 8 m for *P* waves and about 3.8 m for *S* waves. However, most errors are expected to be less than 5 m for *P* waves (average velocity about 1.2 km/sec) and less than 2.5 m for *S* waves (average velocity about 0.5 km/sec).

We suggest that the seismic model is fairly accurate (within 0.05 km/sec) with respect to average velocity, but we do not have direct measure of the *S*-wave velocity within the LVZ. The *S*-wave velocity within the LVZ is approximated on the basis of the delay in travel time and attenuation of the *S* wave. Thus, local variations in velocity structure are not as well resolved. Such variations in the velocity structure could be very important. For example, due to the limited length of our seismic array and to our limited volume of data, the *S*-wave LVZ could be modeled as a laterally continuous layer along the east–west line (Fig. 9a) and a locally confined layer along the north–south line (Fig. 9b). However, our preferred model (Figs. 3 and 4), with a locally confined LVZ, is more consistent with our data and the travel time observations of Spudich *et al.* (1996), as discussed below.

Variations in the *S*-wave velocity greatly affect the calculated Poisson's ratios and the layer thickness. The lack of resolution in layer thickness and the lateral ambiguity in velocity structure along the lines are due to a lack of shot points near the center of the line. A center shot point would be particularly desirable because the largest velocity anomalies are apparently beneath the center of the seismic arrays, and there is little control on the near-surface (upper few meters) velocity. Although there is a close correspondence between velocity boundaries in the seismic model and those observed from borehole data (discussed below), we suggest that the velocity structure does not necessarily correspond to lithologic structure because velocity boundaries can be gradational due to weathering and composition, and longer wavelength seismic waves can average the velocities and depths (discussed below).

Correlations with Seismic Records and Modeling

First arrivals correspond to the *P*-wave refracted arrivals that are generally low in amplitude relative to the secondary (*S*-wave) arrivals on horizontal-component records (Figs. 5 through 8). First arrivals, however, were picked from vertical-component records for purposes of accuracy.

For each of the seismic records, we have outlined our interpretation of the major phases corresponding to arrivals from each layer and compared them to calculated arrivals (Figs. 5 through 8). We interpret three travel-time branches on the E–W seismic records for both *P* and *S* waves (Figs. 5 and 6). The *P*-wave arrival progressively increases in velocity across the seismic record, particularly along the E–W line where seismic energy penetrates to greater depths. In contrast, the *S*-wave appears to be delayed in time (up to 0.2

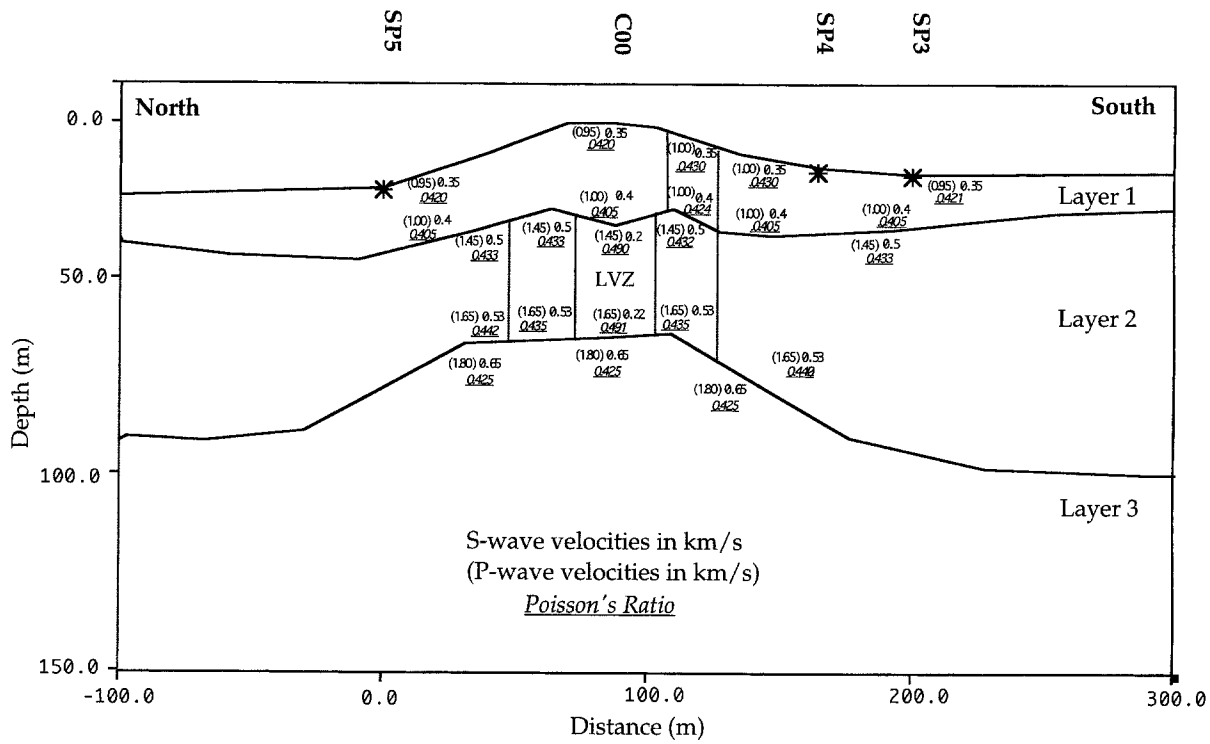

Figure 4. Velocity model (*P* and *S* wave) and Poisson ratio model along the north–south recording array (see Fig. 2). *P*-wave velocities are in parentheses, and Poisson's ratios are underlined. C00 refers to the recording site co-located with the CDMG strong-motion accelerometer. Shot points denoted by SP#. Depth is relative to a datum equal to the highest elevation. Unusually high Poisson's ratios and low *S*-wave velocities are observed within layer 2, beneath the C00 site.

sec) for stations near the C00 site (CDMG site), and the amplitude and frequency of the *S*-wave arrival vary appreciably for stations near the C00 site. The coda at stations near the shot point is fairly simple (e.g., stations 94 to 100 of Fig. 5a and stations 101 to 106 of Fig. 6a); however, the amplitudes, coda, and travel times change appreciably for arrivals beyond the top of the hill (e.g., 101 to 106 of Fig. 5a and 94 to 100 for Fig. 6a). Similar variations in the seismic data are observed on the seismic records from the N–S line (Figs. 7 and 8), but the delay is smaller, and there are fewer observations due to the shorter length of the seismic array.

The first-arrival *P* wave can be picked with ease on all of the seismic records (especially the vertical-component records), but the *S*-wave arrival is assumed to be the high-amplitude secondary arrival. Low-amplitude arrivals between the first arrival and the high-amplitude secondary arrival may be extended coda of the *P*-wave arrival or they may be *S*-wave refractions. We have interpreted these arrivals as extended coda of the *P* waves because they are more readily apparent on vertical-component records than on horizontal-component records. If, however, these arrivals are *S*-wave refractions, then our interpretation of the LVZ would differ, and our estimated value of the *S*-wave velocity within the LVZ may be greater.

A velocity model with a locally confined LVZ produces travel times that are consistent with all of the seismic records (Figs. 5 through 8). The ray diagrams of Figures 5b and 7b demonstrate how a locally confined LVZ can account for the interpreted sections. The interpreted delay in the *S*-wave arrival from layer 2 results from slowing of the seismic waves as they pass through the LVZ, and the frequency and coda of the seismic waves are altered upon entering the locally confined LVZ (Figs. 5a and 7a).

Correlation with Aftershock Analysis

Spudich *et al.* (1996) observed relative travel-time delays and advances across N–S and E–W transects at the Tarzana site. Consistent travel-time delays of approximately 10 ms occurred near the C00 or strong-motion site for wave fields that arrived within 8° of vertical.

We calculated travel times for an upcoming, vertically incident seismic wave field in our model. On both transects, we calculate a maximum delay of about 12 ms (after the effect of topography is removed) near the strong-motion sensor (C00), consistent with the observation of Spudich *et al.* (1996). This delay in travel times near C00 may be indicative of an LVZ that is locally confined to the area near C00, as shown in our preferred model.

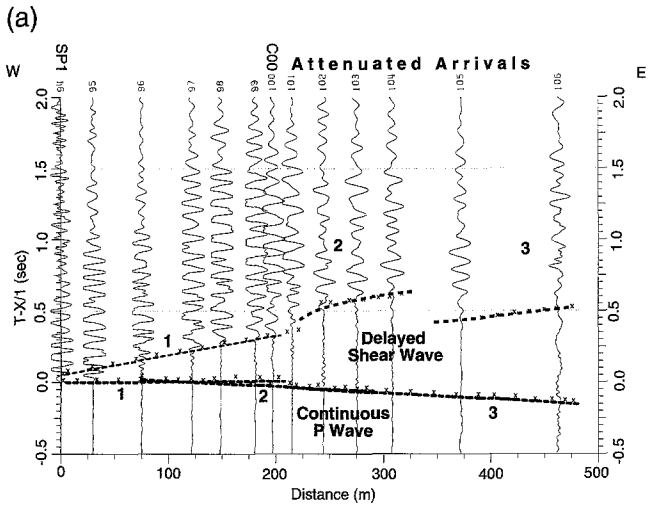

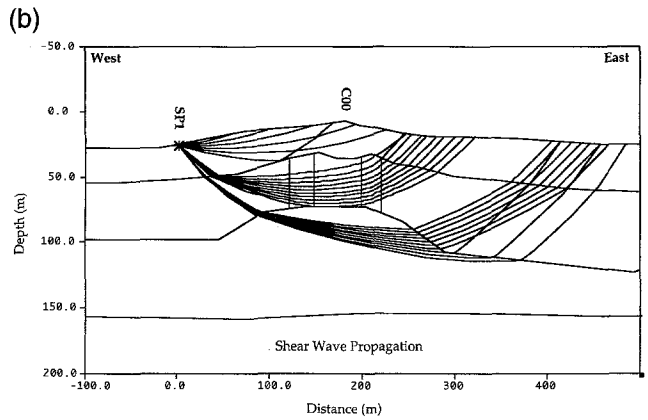

Figure 5. (a) Horizontal-component seismic record, with interpreted phases, along the east–west recording array. Time is reduced by 1.0 km/sec. The shot point was located at SP 1. Note the apparent delayed *S*-wave arrival, continuous *P*-wave arrival, and attenuated frequencies for seismograms east of the C00 site. The numbers, 1 through 3, refer to arrivals from layers 1 through 3 of the seismic model. The "x" on the data refers to calculated *P*-wave (first arrivals) and *S*-wave travel times for the ray paths shown in (b). (b) Ray diagram for *S*-wave rays traced through the seismic model.

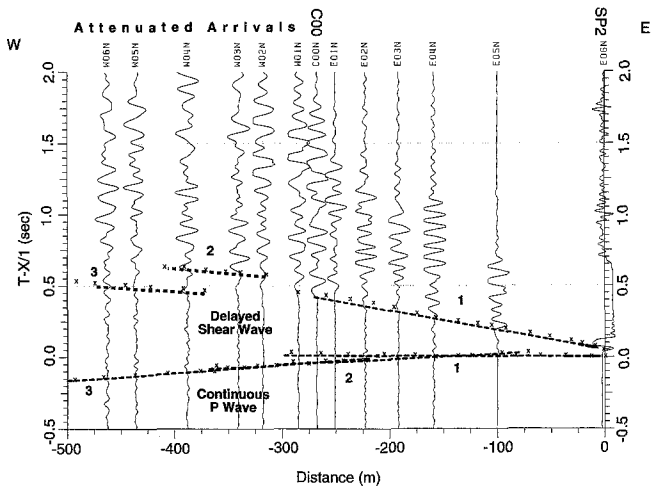

Figure 6. Horizontal-component seismic record, with interpreted phases, along the east–west recording array from shot point 2. Time is reduced by 1.0 km/sec. Note the apparent delayed *S*-wave arrival, continuous *P*-wave arrival, and attenuated frequencies for seismograms west of the C00 site. The numbers, 1 through 3, refer to arrivals from layers 1 through 3 of the seismic model. The "x" on the data refers to calculated *P*-wave (first arrivals) and *S*-wave travel times through the model shown in Figure 3.

Borehole Correlation

Modeled velocities correlate well with the *P*- and *S*-wave velocities measured in a borehole near the base of the hill (Fig. 10a, Fumal *et al.*, 1981). Our velocities compare best with those from the borehole data near the north end of the study area, perhaps because the borehole was located within 100 m of the north end of our N–S array (see Fig. 2). The borehole measurements and the seismic model presented here were made independently, but both yield maximum *P*-wave velocities of about 1.1 km/sec in layer 1 and 1.65 km/sec (Fumal *et al.* calculate 1.66 km/sec from borehole measurements) in layer 2 (Figs. 4 and 10). Fumal *et al.* (1981) calculated borehole *S*-wave velocities to be about 0.38 km/sec in layer 1 (Fig. 10), and the seismic data from our study indicated a range from 0.35 to 0.40 km/sec near the north end of the N–S array (Fig. 4). Using the velocities determined from borehole measurements, the Poisson's ratios are about 0.433 for layer 1 and about for 0.473 for layer 2; both ratios are consistent with those determined from our surface-based measurements.

Fumal *et al.* (1981) noted *P*-wave velocity layering in the upper 30 m that is similar to the layering that we observe along the section of our seismic line nearest to their borehole. They noted a change in *P*-wave velocity from ~1.1 to 1.66 km/sec at about 12 to 15 m in depth (Fig. 10). Similarly, we interpret layer 1 to be about 15 m thick near the north end of our study area (Fig. 4). Fumal *et al.* (1981) did not interpret similar velocity layering for the *S* wave, but we suggest that such layering could be interpreted from their data (Fig. 10). The *S*-wave correlations, as shown in Figure 10, are similar to the velocities determined from our modeling for the upper 30 m.

Assuming our correlation of travel times from Fumal *et al.*'s data, the Poisson's ratios for layers 1, 2, and 3 of Figure 10 are 0.264, 0.410, and 0.467, respectively. Due to our acquisition parameters discussed below, the layer corresponding to a Poisson's ratio of 0.264 is not recognized from our surface-based measurements, but the other two ratios, 0.410 and 0.467, are consistent with the range of Poisson's ratios that we calculated in Figures 3 and 4. The appreciable increase in Poisson's ratio from the surface (0.264) to 25 m (0.467) indicates a change in lithology or a change in physical properties of the rock. Fumal *et al.* (1981) also noted a

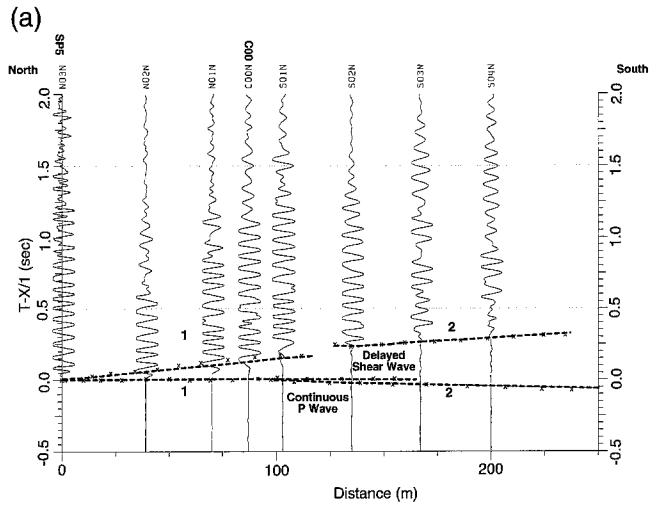

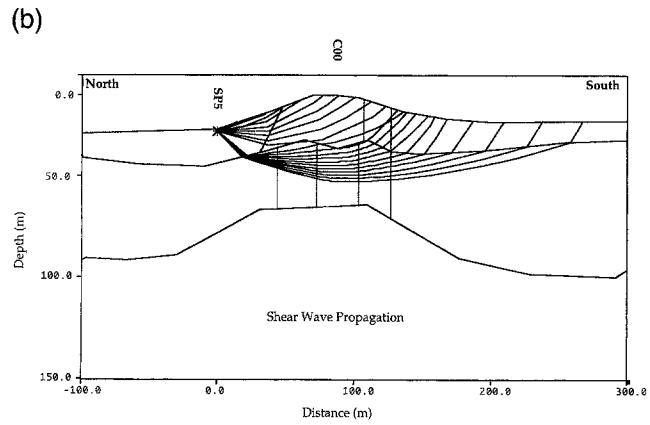

Figure 7. (a) Horizontal-component seismic record, with interpreted phases, along the north–south recording array from shot point 5. Time is reduced by 1.0 km/sec. Note the apparent delayed S-wave arrival, continuous P-wave arrival, and attenuated frequencies for seismograms south of the C00 site. The numbers, 1 and 2, refer to arrivals from layers 1 and 2 of the seismic model shown in Figure 4. The "x" on the data refers to calculated P-wave (first arrivals) and S-wave travel times. (b) Ray diagram for S-wave rays traced through the seismic model.

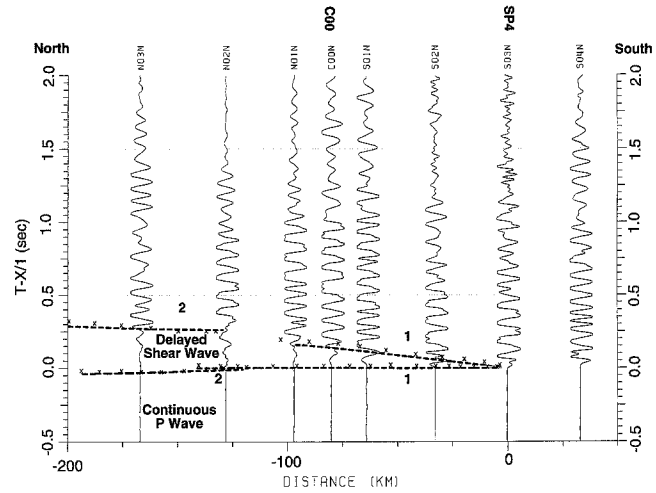

Figure 8. Horizontal-component seismic record, with interpreted phases, along the north–south recording array from shot point 4. Time is reduced by 1.0 km/sec. Note the apparent delayed S-wave arrival, continuous P-wave arrival, and attenuated frequencies for seismograms north of the C00 site. The numbers, 1 and 2, refer to arrivals from layers 1 and 2 of the seismic model shown in Figure 4. The "x" on the data refers to calculated P-wave (first arrivals) and S-wave travel times.

change in physical parameters when they noted a rapid loss in drilling fluid at 24.5 m BGS.

Layer Resolution

As noted above, the velocities and layer thicknesses determined from borehole measurements (Fig. 10) differ only slightly from those that we determined from the explosion-source seismic data (Fig. 4); however, those small differences are less significant when the two sources are compared more closely. The variation in velocities can be attributed in part to the resolution of the two forms of seismic data. The average wavelength of the P wave of our data is about 20 m (where f = 30 Hz, v = (0.83 km/sec + 0.348 km/sec)/2, l = 20 m; where f = frequency, v = velocity, and l = wavelength) if we use the more precise borehole velocities. Thus, our seismic data sampled the subsurface over a depth range of about 20 m, which would include each of the three P-wave velocities (layers of approximate equal thickness) of Figure 10. Because our geophones were spaced about no less than every 15 m and because of the long wavelength of the P wave, the velocity measured in our seismic survey should be an average of the three P-wave velocities of Figure 10. The average velocity determined from the borehole data [(0.348 km/sec + 0.831 km/sec + 1.70 km/sec)/3] is ~0.95 km/sec, and that determined from our surface-based measurements is also 0.95 km/sec at the upper part of the layer.

The average wavelength of the S wave in the first layer is about 6.5 m (v = 0.197 km/sec, f = 30, l = 6.5 m), approximately 11 m in the second layer (v = 0.325 km/sec, f = 30 Hz, l = 10.8 m), and about 14 m (v = 0.420 km/sec, f = 30 Hz, l = 14 m) in the third layer. Due to the minimum 15-m spacing of our geophones and the 6.5-m wavelength of the S wave, the first S-wave layer would not be detected, but the second layer would be averaged with the first layer [(0.325 km/sec + 0.420 km/sec)/2 = ~0.372 km/sec]. Such averaging yields approximately the same average velocity for layer 1 that we determined from our modeling [(0.350 km/sec + 0.400 km/sec)/2 = 0.375 km/sec] along the N–S line.

We suggest that our measurements represent an average of the velocities measured within the borehole, with the S waves delineating the layering at higher resolutions. Greater resolutions are obtained from the borehole data; however, (1) the borehole data represent a point measurement and

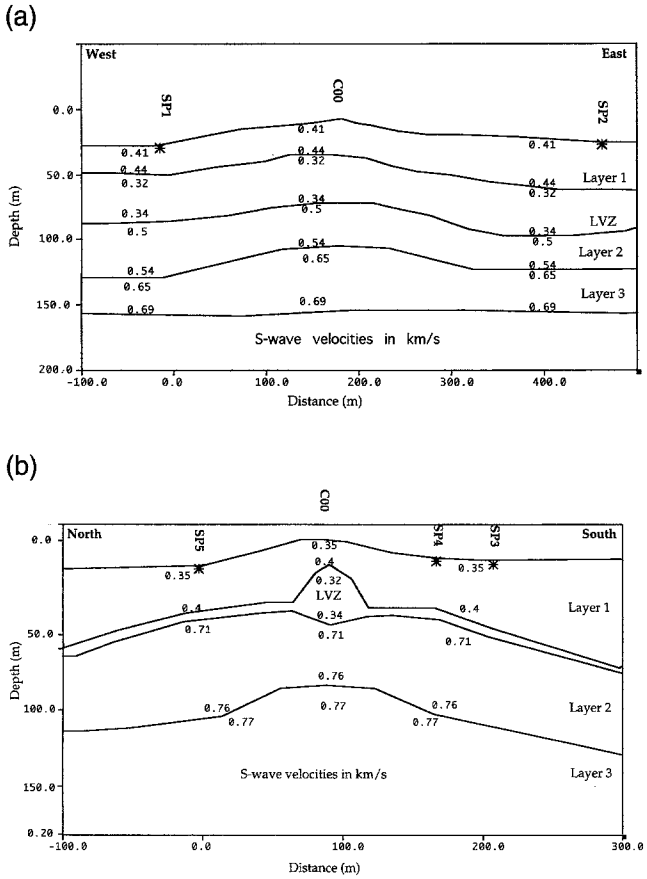

Figure 9. (a) Alternative *S*-wave seismic velocity model with a laterally continuous low-velocity zone (LVZ) along the east–west line. (b) Alternative *S*-wave seismic velocity model along the north–south line. A thick, laterally continuous LVZ is inconsistent with the observed data in the north–south direction. Depth is relative to a datum equal to the highest elevation along each profile.

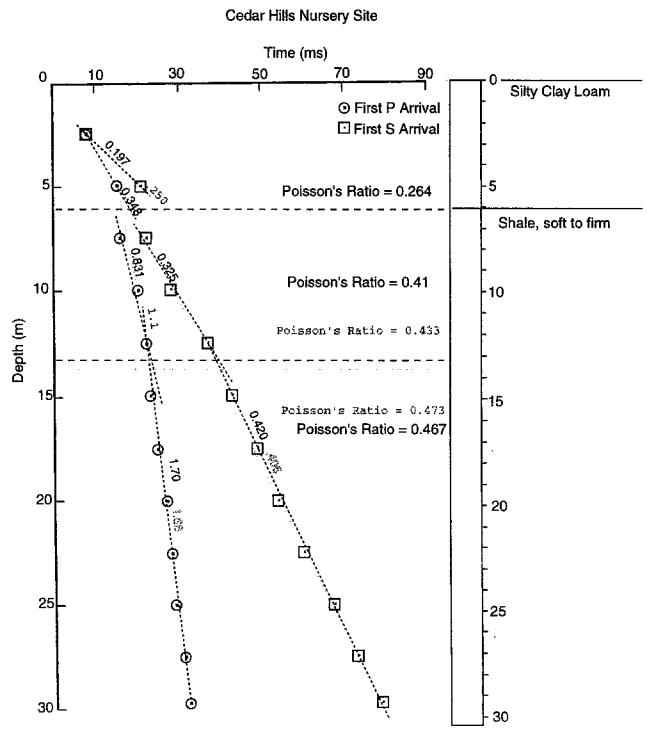

Figure 10. A plot of measured travel times and depths from a borehole drilled at the base of the hill (Fumal *et al.*, 1981; see Fig. 2). The interpreted lithology, Poisson's ratio (light shaded), and velocity determinations (light shaded) are from Fumal *et al.* (1981). The velocity correlations (darker lines and print) and Poisson's ratios (darker print) are based on our reinterpretation of Fumal *et al*'s data.

yield little information about lateral variations, (2) explosion-source measurements are more consistent in wavelength and frequencies with the earthquake-source data, and (3) the explosion-source measurements can be more readily and economically acquired. Thus, in many cases, site-response characteristics may be better modeled on the basis of the longer-wavelength, explosion-source data.

Discussions and Conclusions

Nearby borehole data (Fumal *et al.*, 1981) and outcrops of exposed strata along our seismic lines indicate the Tarzana strong-motion site is underlain by a few meters of silty clay loam at the surface and by an undetermined thickness of soft to firm shale. The borehole data can be interpreted to indicate at least three *P*- and *S*-wave velocity boundaries in the upper 30-m BGS (Fig. 10); two of the layers correlate with changes in the weathering state of the rocks.

Our data are consistent with the borehole data and indicate that the *P*-wave velocities are variable along the seismic line in the upper 25-m BGS. The *P*-wave velocities do not appear to be anomalous near the CDMG strong-motion site; however, the *S*-wave velocities appear to be appreciably lower beneath the CDMG site in layer 2. The observed variations in the *S*-wave velocities and frequencies, coupled with a lack of similar variations in the *P*-wave velocities and frequencies, may indicate that the zone beneath about 25-m BGS at the top of the hill is cavernous, largely saturated, or a combination of both. The rapid loss in drilling fluid at a nearby drill site by Fumal *et al.* (1981) may indicate that there are large open spaces at those depths, but it is unlikely that such open spaces persist over a large region. Hollow spaces in the subsurface could account a shear-wave LVZ, but the *P* wave would also decrease in amplitude and velocity. A saturated subsurface, however, could account for the velocity and amplitude attenuation observed.

The effect of water saturation on *P*- and *S*-wave velocities (Nur, 1982) is demonstrated in Figure 11. Water-saturated sedimentary rock is lower in *P*- and *S*-wave velocities relative to dry sedimentary rock, except near 100% saturation. At nearly 100% saturation, the *P*-wave velocity is high, but the *S*-wave velocity is low relative to dry samples. The data from Figure 11 suggest that Poisson's ratios at satura-

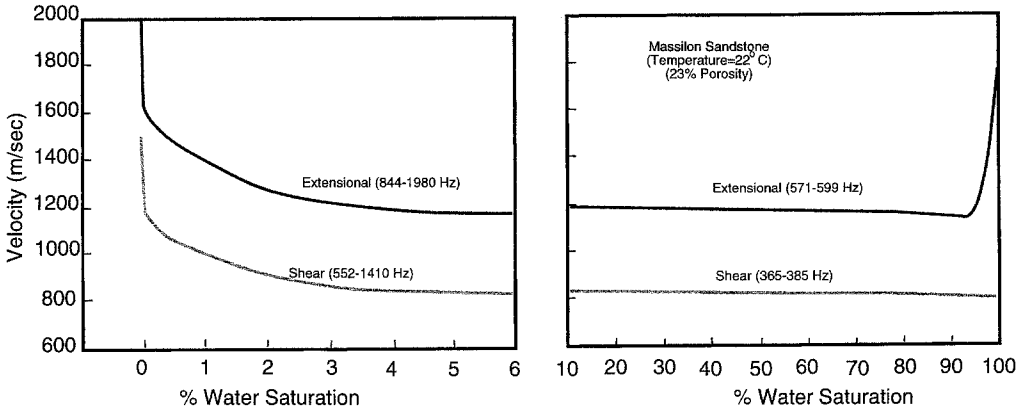

Figure 11. Velocity of Massilon sandstone as a function of the percentage water saturation (from Nur, 1982). Note that velocities decrease with greater saturation until nearly 100% saturation, where P-wave velocities greatly increase.

tion levels of 1, 50, 97, and 100% in Massilon sandstone are 0.332, 0.414, 0.461, and 0.484, respectively. The maximum Poisson's ratio calculated for the shallow subsurface beneath the Tarzana site is 0.491, which is greater than the values calculated for Massilon sandstone at saturation levels near 100%. The rocks at Tarzana are shales, not sandstones as in Figure 11; and at shallow depths, shales are typically more porous (20 to 39%) than Massilon sandstone (22%) (Clark, 1966). The greater porosity of shale may indicate higher fluid content of the rocks at Tarzana, accounting for the high Poisson's ratios.

Fumal *et al.* (1981) calculated Poisson's ratios for a number of sites around the Los Angeles area using velocities determined from borehole measurements. They found that most "wet" shale samples had Poisson ratios between 0.47 and 0.49, which includes the range of ratios we estimate for the Tarzana site below depths of below 40 m. However, the dry samples of Fumal's *et al.* study typically had Poisson's ratios between 0.15 and 0.35. A high degree of saturation at the Tarzana site is also consistent with the observed attenuation of higher frequencies in our seismic data (Figs. 5 through 8) because S-wave attenuation of refracted waves is high at near-100% saturation, but P-wave attenuation of refracted waves is relatively low at near-100% saturation (Nur, 1982; Fig. 12).

We suggest that such a saturated zone beneath the top of the hill at the Tarzana site may also account for the exaggerated shaking that is locally confined to the top of the hill. Such strong shaking apparently did not occur at distances as little as 150 m from the CDMG (C00) site because stacked clay pottery remained intact and mobile homes, perched on wooden pillars, were not toppled. Strong shaking near the CDMG site is, however, indicated by more than the

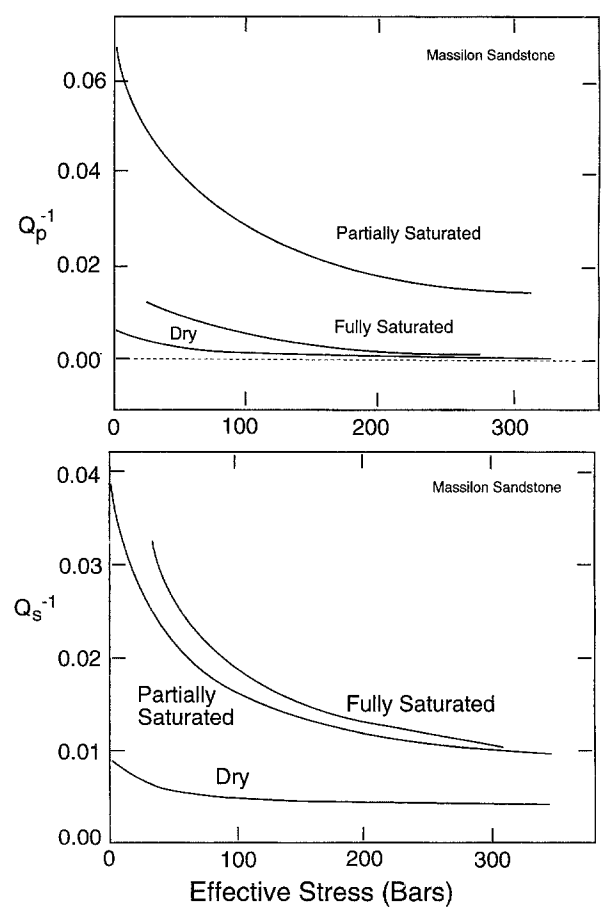

Figure 12. Attenuation of seismic waves as a function of the degree of water saturation (from Nur, 1982). Note that attenuation of S-waves at ~100% saturation is high relative to P waves.

CDMG accelerometer, as the house near the site (see Fig. 2) was severely damaged during the Northridge earthquake. Aftershock data of Lee *et al.* (1994) also indicate that the highest amplitudes generally occurred within about 75 m of the CDMG site. Apparently a 100- to 150-m-wide saturated zone correlates with the dimensions of the strongest shaking. Such a saturated zone may also explain the high-amplitude, lower-frequency *S*-wave arrivals and extended coda seen in Figures 5 through 8. Our modeling results are also consistent with Spudich *et al.*'s (1996) conclusion that the internal structure of the hill is likely a significant contributor to the strong skaking observed at Tarzana.

We do not know if or why there should be a saturated zone beneath the top of the hill at the Tarzana site, but perhaps extensive watering of the lawn and the nursery at the Tarzana estate over the past half century may have caused saturation. Alternatively, fluids may be naturally occurring within the core of the small hill, as naturally occurring springs are observed in the area near the base of the hill (P. Spudich, personal comm., 1995), consistent with saturation.

Although our data are consistent with a saturated zone and a low-velocity zone for *S* waves beneath the top of the hill, we do not regard our data and interpretation as conclusive. A much more detailed seismic investigation with denser wave-field sampling, denser shot-point spacing, and borehole measurements is needed to improve the resolution. If highly saturated rocks exist beneath the surface of the Tarzana site and such conditions exist elsewhere, local strong ground shaking on topographically high sites may be a hazard in numerous other localities. Because many structures are typically placed on top of topographic highs in urban areas and because these "hard-rock" sites are often considered safer building areas, the determination of any possible hazard associated with such sites may be particularly important.

Acknowledgments

We thank R. A. White, D. H. Harlow, J. A. Rodgers, J. Hamilton, C. Garvin, J. O. Catchings, B. F. Catchings, Jr., A. Kolesnikov, A. Ross, and J. Gibbs for field assistance, Ralph J. Herman for permitting us to conduct the survey on his property, Bernard Chouet for lending equipment, J. Mori for funding the investigation, and A. Lindh for suggesting the investigation and for administrative assistance. We thank Paul Spudich, G. S. Fuis, and the BSSA reviewers for reviewing the manuscript.

References

Cerveny, V., I. A. Molotkov, and I. Psencik (1977). *Ray Method in Seismology,* Charles University Press, Prague, 214 pp.

Clark, S. P., Jr. (Editor) (1966). *Handbook of Physical Constants, Geol. Soc. Am. Mem. 97,* New York, 587 pp.

Dibblee, T. W. Jr. (1992). Geologic map of the Topanga and Canoga Park (South 1/2) Quadrangles, Los Angeles County, California, Map DF-35, Dibblee Geol. Foundation, Santa Barbara, California.

Fumal, T. E., J. F. Gibbs, and E. F. Roth (1981). In-situ measurements of seismic velocity at 19 locations in the Los Angeles, California region, *U.S. Geol. Surv. Open-File Rept. 81-399.*

Hoots, H. W. (1931). Geology of the eastern part of the Santa Monica Mountains, Los Angeles County, California, *U.S. Geol. Surv. Profess. Paper 165-C,* 134 pp.

Lee, W. H. K. (Editor) (1989). Toolbox for Seismic Data Acquisition, Processing, and Analysis, IASPEI Software Library, Vol. 1, Seis. Soc. Am., El Cerrito, California, 278 pp.

Lee, W. H. K. and D. A. Dodge (Editors) (1992). A course on: PC-based seismic networks, *U.S. Geol. Surv. Open-File Rept. 92-441,* 535 pp.

Lee, W. H. K., R. A. White, D. H. Harlow, J. A. Rogers, P. Spudich, and D. A. Dodge (1994). Digital seismograms of selected aftershocks of the Northridge earthquake recorded by a dense seismic array on February 11, 1994 at Cedar Hill Nursery in Tarzana, California, *U.S. Geol. Surv. Open-File Rept. 94-234.*

Lui, Hsi-Ping, R. E. Warrick, R. E. Westerlund, J. B. Fletcher, and G. L. Maxwell (1988). An air-powered impulsive shear-wave source with repeatable signals, *Bull. Seism. Soc. Am.* **78,** 355–369.

Luetgert, J. H. (1988). User's manual for MacR1D84 Interactive Modeling of 1-D velocity depth-functions, *U.S. Geol. Surv. Open-File Rept. 88-247,* pp. 30.

Luetgert, J. H. (1992). Interactive two-dimensional seismic raytracing for the Macintosh, *U.S. Geol. Surv. Open-File Rept. 92-356,* 43 pp.

Nur, Amos (1982). Stanford Rock Physics Progress Report, January 1982, Vol. 13, Stanford Junior University, Stanford, California, 121 pp.

Shakal, A., M. Huang, and T. Cao (1988). The Whittier Narrows, California, earthquake of October 1, 1987: CSMIP strong motion data, *Earthquake Spectra* **4,** 75–100.

Shakal, A., M. Huang, R. Darragh, T. Cao, R. Sherburne, P. Malhotra, C. Cramer, R. Sydnor, V. Graizer, G. Maldonado, C. Peterson, and J. Wampole (1994). CSMIP strong-motion records form the Northridge, California earthquake of 17 January 1994, Report No. OSMS 94-07, California Division of Mines and Geology, Sacramento, California, 308 pp.

Spudich, P., Hellweg, and W. H. K. Lee (1996). Directional topographic site response at Tarzana observed in aftershocks of the 1994 Northridge, California, earthquake: implications for main shock motions, *Bull. Seis. Soc. Am.* **86,** S193–S208.

U.S. Geological Survey
345 Middlefield Rd., MS 977
Menlo Park, California 94025

Manuscript received 20 October 1995.